Polym. Bull. (2012) 69:15–28
DOI 10.1007/s00289-011-0685-7

ORIGINAL PAPER

Effect of silane-modified ZnO on morphology and properties of bionanocomposites based on poly(ester-amide) containing tyrosine linkages

Amir Abdolmaleki · Shadpour Mallakpour · Sedigheh Borandeh

Received: 16 August 2011 / Revised: 13 November 2011 / Accepted: 27 November 2011 /
Published online: 10 December 2011

Abstract In this study, various optically active poly(ester-amide)/Zinc oxide bionanocomposites (PEA/ZnO BNCs) were synthesized with different amount of modified ZnO nanoparticles using ultrasonic irradiation. To obtain the homogeneous distribution of ZnO in polymer matrix, the surface of nanoparticles was modified to organophile with γ-aminopropyltriethoxyl silane. PEA/ZnO BNCs were characterized by Fourier transform infrared spectra, X-ray diffraction, field emission scanning electron microscopy (FE-SEM), atomic force microscopy (AFM), and transmission electron microscopy (TEM). The FE-SEM, AFM, and TEM results confirmed that the nanoparticles were dispersed uniformly in PEA matrix at the nanoscale. In addition, thermogravimetric analysis data indicated an improvement of thermal stability of novel BNC materials as compared to the pure polymer.

Keywords Poly(ester-amide) · Zinc oxide · Ultrasonic irradiation · Atomic force microscopy (AFM)

A. Abdolmaleki (✉) · S. Borandeh
Department of Chemistry, Isfahan University of Technology, 84156-83111 Isfahan, Islamic Republic of Iran
e-mail: abdolmeleki@cc.iut.ac.ir; amirabdolmaleki@yahoo.com

A. Abdolmaleki · S. Mallakpour
Nanotechnology and Advanced Materials Institute, Isfahan University of Technology, 84156-83111 Isfahan, Islamic Republic of Iran

S. Mallakpour (✉)
Organic Polymer Chemistry Research Laboratory, Department of Chemistry, Isfahan University of Technology, 84156-83111 Isfahan, Islamic Republic of Iran
e-mail: mallak@cc.iut.ac.ir; mallak777@yahoo.com; mallakpour84@alumni.ufl.edu

Introduction

The best candidate to be hosting matrices for composite materials is polymers due to their ability to yield a variety of properties. Furthermore, organic polymers generally have long-term stability and good flexibility [1, 2]. However, polymers have some disadvantages such as poor thermal and electrical properties and have lower modulus and strength in comparison with metals and ceramics. Different ways, such as synthesis of homopolymers, copolymers, and modified polymers were performed but they were not sufficient to compensate various properties, which were required. On the other hand, inorganic nanoparticles possess excellent optical, catalytic, electronic, and magnetic properties [3–7]. By combining these two components, nanocomposites derived from organic polymers and inorganic nanoparticles are expected to improve properties [8–12]. In general, these resulting organic polymer-based inorganic nanoparticle composites have been used in various fields such as electronics, coatings, and catalysis [13–16].

The aggregation of inorganic nanoparticles in polymeric matrix is one of the limitations of the applications of polymer-inorganic nanocomposites. To prevent the incompatibility in surface properties and to achieve a homogeneous distribution of inorganic particles without aggregation, the surface of particles must be modified with suitable compatibilizers [17–19]. Coupling agents have gained more attention because of their individual structures, which have two different functional groups, one side is compatible with polymer matrix and the other is bonded to the surface of inorganic nanoparticle. One of the most popular and applicable coupling agents is silane coupling agents. The coupling process can be accomplished via the chemical reaction between the trialkoxy groups of silane molecules and the hydroxyl groups on the nanoparticles, whereas other functional groups of silane molecules, which are generally ethylene, amine, epoxy, thiohydroxy, etc., remain intact [20–22].

In the choice of polymeric matrix, several properties such as chemical stability, bio-compatibility, and chemical functionalities should be examined. Poly(ester-amide)s (PEA)s can be a good candidates for these purposes because of their significant properties such as high temperature stability, mechanical strength, good chemical resistance, high biodegradability, and flexibility [23, 24]. In addition, incorporating α-amino acids into their backbones causes to have chiral property and improves the biodegradability properties of these polymers [25–28].

Among various nanoparticles with different properties and applications, ZnO with hexagonal wurtzite structure, is one of the multifunctional inorganic semiconductors [29] that has drawn increasing attention in recent years due to its many significant potential application in solar cells [30], gas sensors [31], varistors [32], piezoelectric devices, electro-acoustic, transducers, chemical absorbent [33], UV light emitting devices [34], sun-screens, UV absorbers [35], and electrostatic dissipative coating [36]. Furthermore, ZnO is an environmentally friendly material and has little toxicity, which is desired for bio-applications [37].

In the present investigation, an optically active and biodegradable PEA was used as a polymer matrix. The ZnO nanoparticles were treated with coupling agent of γ-aminopropyltriethoxyl silane (KH550) to introduce organic functional groups on the surface of ZnO and improve the dispersion of nanoparticles. Then novel

optically active PEA/zinc oxide bionanocomposites (PEA/ZnO BNCs) were synthesized under ultrasonic irradiation conditions. The resulting BNCs were characterized by various techniques including FT-IR, X-ray diffraction (XRD), TGA, Differential scanning calorimetry (DSC), and their morphology were investigated by field emission scanning electron microscopy (FE-SEM), atomic force microscopy (AFM), and transmission electron microscopy (TEM) analysis.

Experimental

Materials

S-Tyrosine was purchased from Merck Chemical Co. *N*-methyl-2-pyrrolidinon (NMP, Merck Chemical Co.) and triethylamine (Merck Chemical Co.) were dried over BaO and then were distilled under reduced pressure and stored over 4-Å molecular sieves. Isophthaloyl dichloride (**2**) (Merck chemical Co.), and other reagents and solvents were obtained commercially and used as received. ZnO nanoparticle with an average particle size of about 25–30 nm was purchased from Neutrino Co. The silane coupling agent (KH550) was purchased from Merck Chemical Co.

Characterizations techniques

The chemical composition of the intermediates and obtained particles was studied by FT-IR spectroscopy using a Jasco-680 FT-IR spectrophotometer (Japan) in the spectral range between 4,000 and 400 cm^{-1} with KBr pellet. Vibration bands were reported as wave number (cm^{-1}). The band intensities are assigned as weak (w), medium (m), shoulder (sh), strong (s), and broad (br). The XRD patterns were recorded by using a Philips Xpert MPD diffractometer equipped with a Cu Kα anode ($\lambda = 1.5418$ Å) in 2θ range of 10°–80° at the speed of 0.05° min^{-1}. UV/vis spectra were measured on UV/Vis/NIR spectrophotometer, JASCO, V-570 with solid pellets of the samples in the spectral range between 200 and 800 nm. Thermal properties of polymer and nanocomposites were studied on STA503 win TA instrument in nitrogen atmosphere at a heating rate of 10 °C min^{-1}. DSC analysis was taken by Perkin-Elmer DSC-7 in nitrogen atmosphere at a heating rate of 10 °C min^{-1}. FE-SEM micrographs of samples were taken on a Hitachi (S-4160). AFM topographic images were obtained using Digital Multimode Instruments Nanoscope III (Digital Instrument Inc., USA) with noncontact tapping mode with a silica probe (NSC 11) and a frequency of 463 kHz. The morphology and dispersity analysis was performed on TEM analyzer on Philips CM 120 operating at 100 kV. The reaction was carried out on a Misonix ultrasonic liquid processor, XL-2000 Series. Ultrasound was a wave of frequency 2.25×10^4 Hz and power 100 W.

Monomer synthesis

N,N′-Bis[2-(methyl 3-(4-hydroxyphenyl)propanoate)] isophthaldiamide (**3**) was synthesized via the reaction of *S*-tyrosine methyl ester (**1**) [38] (1.07 g, 5.5 mmol)

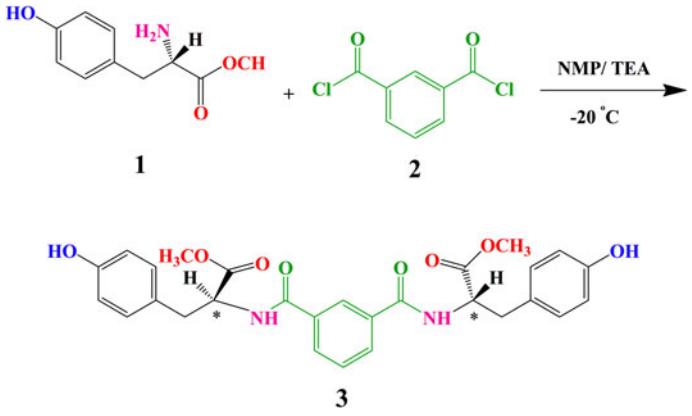

Scheme 1 Synthesis of diol **3**

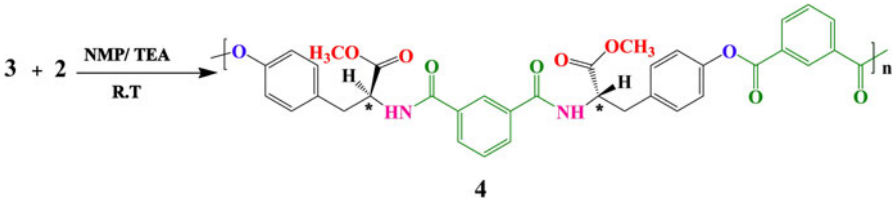

Scheme 2 Synthesis of PEA

and isophthaloyl dichloride (**2**) (0.5 g, 2.5 mmol) in 6 mL of NMP as a solvent at −20 °C (Scheme 1) [39].

Synthesis of PEA

PEA was synthesized via polycondensation of diol **3** with isophthaloyl dichloride **2** (Scheme 2) [39].

Surface modification of ZnO nanoparticles

ZnO nanoparticle was dried at 110 °C for 24 h to remove absorbed water. ZnO nanoparticle (0.2 g) was added into absolute ethanol (10 mL) and was ultrasonicated for 15 min. Then, 0.042 mL of KH550 (20 wt% ZnO) was added to the dispersed solution. The mixture of nanoparticles and KH550 was irradiated under ultrasonic radiation for 30 min, after which the suspension was filtrated and washed with ethanol to remove unreacted KH550. The solid was dried at 60 °C for more than 24 h.

Preparation of PEA/ZnO BNCs

The preparation of PEA/ZnO BNCs was carried out by the following procedure: Different amounts of modified ZnO nanoparticles (2, 4, 6, 8, and 10 wt%) were

mixed with PEA (0.1 g) and the mixture was dispersed in 20 mL of absolute ethanol and then was irradiated under ultrasound waves for 4 h. The solvent was removed and the obtained solid was dried in vacuum at 80 °C for 4 h.

Results and discussion

Surface modification of ZnO nanoparticles

Surface-treating ZnO filler with a suitable modifying agent can improve the compatibility of ZnO filler with polymer matrix, promotes effectively the adhesion of polymer matrix to ZnO filler; and reduces the aggregation of nanoparticles in polymer/ZnO nanocomposite. In this study, the surface of ZnO nanoparticles was treated using KH550. A substitution reaction can take place between the hydroxyl surface groups of the ZnO nanoparticles and the $-OCH_2CH_3$ groups from the coupling agent, thereby changing the ZnO surface to be more hydrophobic with better affinity to organic matrix. The modified ZnO nanoparticles also provide steric hindrance between inorganic nanoparticles and organic polymer that support uniform dispersion and prevent aggregation. For coupling agent KH550, the functional group that provides different interactions to ZnO nanoparticle is the amino group. Various interaction types between aminosilane and ZnO surface were proposed as follows: (a) hydrogen bonding, (b) ionic bonding, and (c) covalent bonding with surface hydroxyl groups [40–42]. The details of the mechanism are shown in Fig. 1.

Structure study

The X-ray diffraction patterns of pure PEA, ZnO nanoparticle and PEA/ZnO BNCs (6, 8, and 10 wt%) over the 2θ range of 10°–80° are shown in Fig. 2. Based on XRD pattern of pure PEA, it is clear that this polymer is totally amorphous in nature and does not show any sharp diffraction peaks. The XRD patterns of ZnO nanoparticles show hexagonal wurtzite structure. The characteristic peaks are observed at 31.8

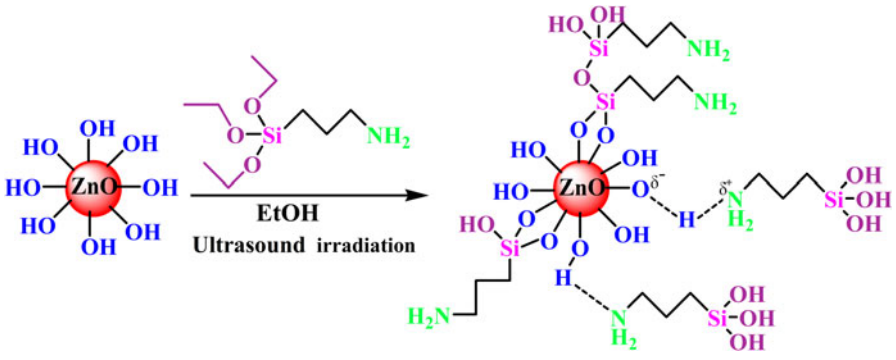

Fig. 1 Surface modification of ZnO nanoparticles with KH550

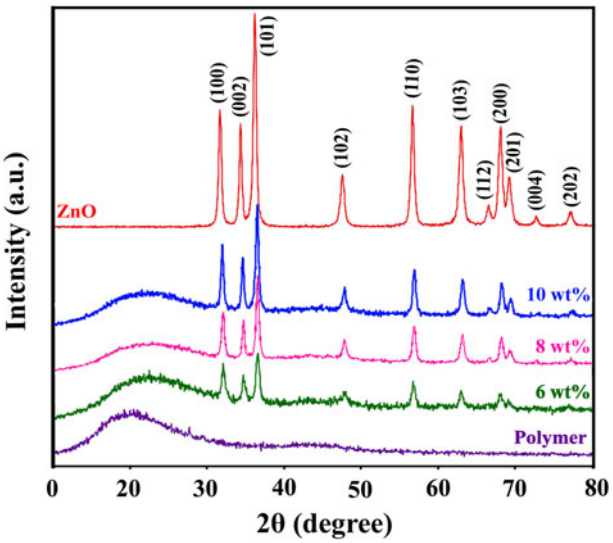

Fig. 2 XRD curves of pure PEA, pure ZnO nanoparticles, and PEA/ZnO BNCs (6, 8, and 10 wt%)

(100), 34.4 (002), 36.2 (101), 47.6 (102), 56.6 (110), 62.9 (103), 66.4 (200), 67.9 (112), 69.1(201), 72.6 (004), and 77.0 (202). All the diffraction peaks are in agreement with JCPDS data (No. 36-1451). The XRD of the BNCs have similar pattern as that of ZnO powder and characteristic amorphous contribution of the polymer at lower 29 values.

The crystallite size of ZnO in BNCs was found to be 28–32 nm as calculated from the three peaks using the Scherrer formula ($D = K\lambda/\beta\cos\theta$), where D is the average crystallite size, K is the Scherrer constant (0.9), λ is the wave length of Cu (1.54 Å), β is the full width of diffraction line at half-maximum intensity, and θ is the Bragg angle.

FT-IR analysis

The structure of modified ZnO and synthesized BNCs were confirmed by FT-IR spectroscopy as shown in Figs. 3b and 4, respectively. In the spectrum of pure ZnO nanoparticle (Fig. 3a), the existence of a broad peak at 3,434 cm^{-1} confirms the OH groups on the surface of ZnO. The broad and high intensity peak near 430 cm^{-1} is pointed to Zn–O bond stretching. The spectrum of functionalized ZnO with KH550 (Fig. 3c) showed new peaks as compared to pure ZnO. The bands at 2924, 2889, and 2856 cm^{-1} assigned to C–H asymmetrical stretching vibration (CH_3 group), C–H asymmetrical stretching vibration (CH_2 group), and C–H symmetrical stretching vibration (CH_2 group) are detected. In this spectrum, the bands at 2,889 and 2,856 cm^{-1} were assigned to alkyl groups [–$(CH_2)_n$–], but their intensities are rather weak. The N–H bending vibration of primary amine is appeared at approximately 1,578 cm^{-1}. In addition, the broad band appears around 1,509 cm^{-1}. This examination revealed that the band corresponding to NH_2 deformation mode

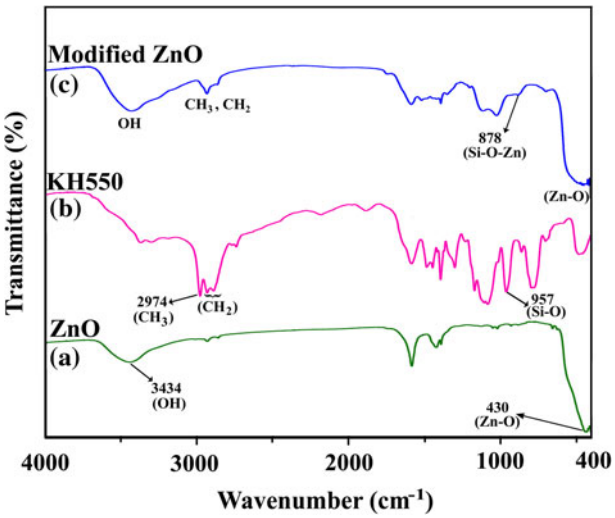

Fig. 3 FT-IR spectra of (*a*) pure ZnO nanoparticles, (*b*) KH550, and (*c*) ZnO nanoparticles functionalized by KH550

shifted to lower wave number due to interaction with silanol group or surface hydroxyl groups of ZnO. Furthermore, the peaks at 1017, 878, and 444 cm^{-1} were assigned to Si–O–Si, Zn–O–Si, and Zn–O bonds, respectively. The appearance of these bands proves that functional groups in silane coupling agent (propyl or aminopropyl group, etc.) are attached on the surface of ZnO nanoparticles.

The FT-IR spectra of pure PEA and BNCs are shown in Fig. 4. According to this figure, pure PEA has characteristic peaks at 3408 (N–H), 1741 (C=O ester), 1663 (C=O amide), 1299 (C–N), and 1221 (C–O) cm^{-1}. The FT-IR spectra of BNCs show the characteristic peaks of both pure PEA and ZnO nanoparticles. From these spectra, it is reasonable that with increasing the amount of nanoparticles the intensity of absorption related to Zn–O–Zn bonds was enhanced.

Morphology study

The dispersion quality of the nanoparticles within the PEA matrix was investigated by FE-SEM and AFM. Figure 5 shows the FE-SEM micrographs of PEA/ZnO BNC (10 wt%). The FE-SEM images of PEA/ZnO BNC (a, b) reveal that the ZnO nanoparticles were homogeneously dispersed in the PEA matrix and the average particle size of the nanoparticles was in the range of 35–66 nm (Fig. 5c). Due to treating ZnO filler with modifying agents such as KH550, the compatibility of ZnO filler with PEA matrix are able to be improved. In addition, ultrasound irradiation effect on the distribution and particle size of the nanoparticles.

AFM was utilized to investigate the morphology (shape and size) of PEA/ZnO BNC (10 wt%) (Fig. 6a, b). The AFM images of PEA/ZnO BNC also agree with the observation in FE-SEM images. It is noteworthy that no aggregation of ZnO nanoparticle can be seen in polymer matrix (Fig. 6a). The AFM image reveals a

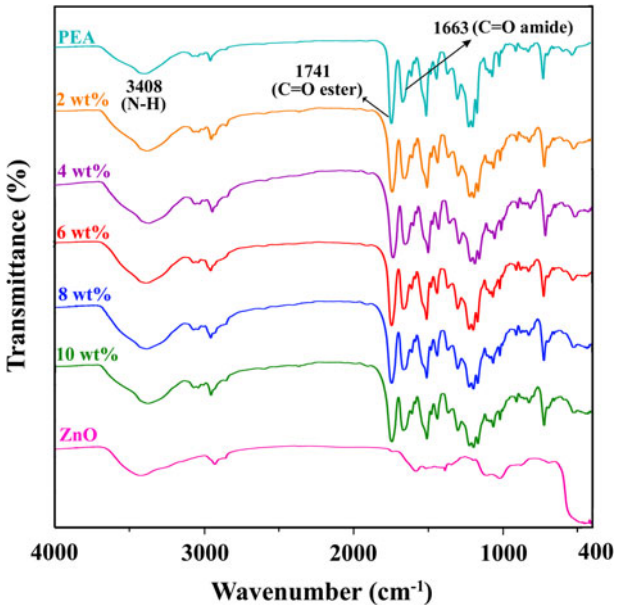

Fig. 4 FT-IR spectra of modified ZnO, pure PEA, and PEA/ZnO BNCs

uniform dispersion of spherical shaped particles throughout the PEA/ZnO NBC. The observed dimensions are below 100 nm.

In addition, TEM micrographs of PEA/ZnO BNC (10 wt%) (Fig. 7) confirmed good and homogeneous dispersion of ZnO naoparticles into PEA matrix. It is obviously seen that the mean diameter of particles is in the range of 30–50 nm. From this data it is found that modifying ZnO nanoparticles with silane coupling agent has an important role on the dispersion of nanoparticles. Proper functionalization of the nanoparticles, improves their compatibility with polymer matrix. Here, the functional group is NH_2, which can lead to hydrogen bonding with the esteric or amidic C=O and N–H groups in PEA. Other participating interactions may arise between the unmodified OH groups of ZnO surface and these functional groups in PEA through H-bonding. The details are shown in Fig. 8.

UV/Vis absorption

The optical properties of pure PEA, modified ZnO, and PEA/ZnO BNCs were examined and were shown in Fig. 9. According to these spectra, the maximum absorption peak of pure PEA and modified ZnO nanoparticle appeared at 400 and 368 nm, respectively. These peaks in the UV/Vis range correspond to π–π^* transitions and to the polaronic transitions ($n \rightarrow \pi^*$ transitions). The maximum absorption peak of BNCs shifted to the maximum absorption peak of modified ZnO and the peaks became broader with a shoulder with increasing ZnO content. As a result, these BNCs could be used as UV-shielding materials due to their absorption in UV region.

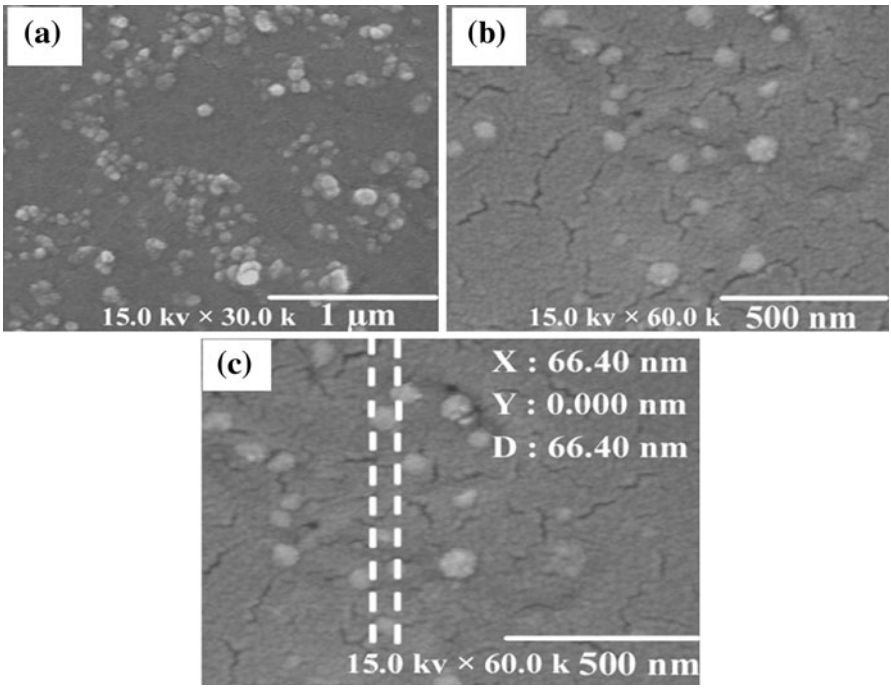

Fig. 5 FE-SEM micrographs of PEA/ZnO BNC (10 wt%)

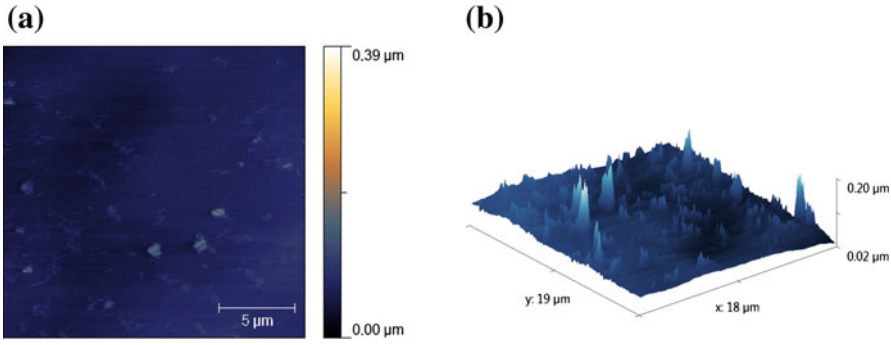

Fig. 6 The two and three dimension AFM topography images of PEA/ZnO BNC (10 wt%)

Thermal properties

The TGA spectra of pure PEA, PEA/ZnO BNCs (6, 8, and 10 wt%), and the resulting data are shown in Fig. 10 and Table 1, respectively. As shown in the figure, the T_5 and T_{10} wt% increase with the increasing ZnO contents and the char yields of BNCs at 800 °C improve with increasing ZnO content. The increasing in thermal stability of BNCs may be due to the good compatibility of modified ZnO

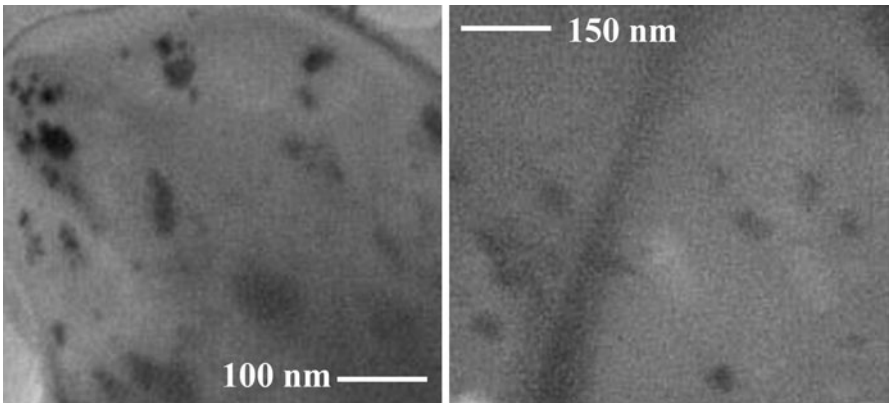

Fig. 7 TEM micrographs of PEA/ZnO BNC (10 wt%)

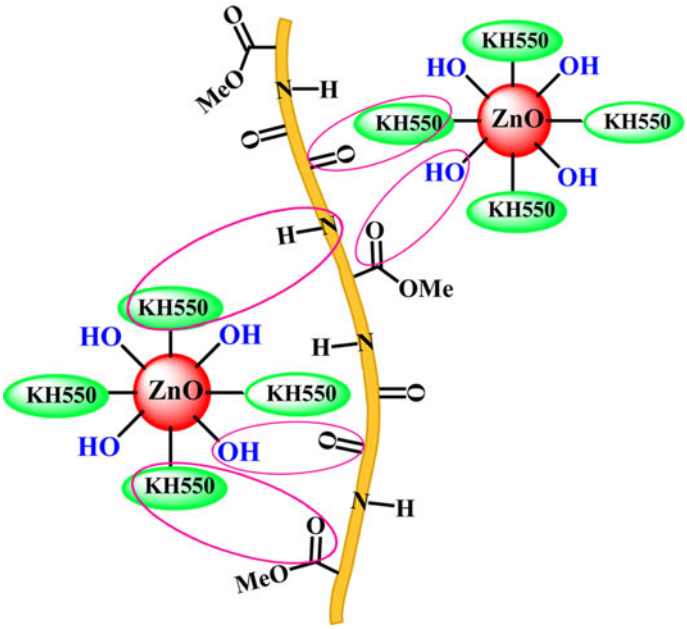

Fig. 8 The mechanism of PEA/ZnO BNC formation

nanoparticles with polymer matrix. ZnO nanoparticles have high thermal stability because of their larger surface area, so the incorporation of ZnO nanoparticles can improve the thermal resistance of the obtained BNCs. Also the limiting oxygen index (LOI) of pure PEA and BNCs was calculated (LOI = 17.5 + 0.4 CR, where CR is char yield) [43] and reported in Table 1.

The DSC thermograms of pure PEA, pure PEA which was ultrasound, and PEA/ZnO-KH550 (10 wt%) are shown in Fig. 11. As shown in the figure, the glass transition temperature (T_g) of the polymer was decreased after ultrasonication and

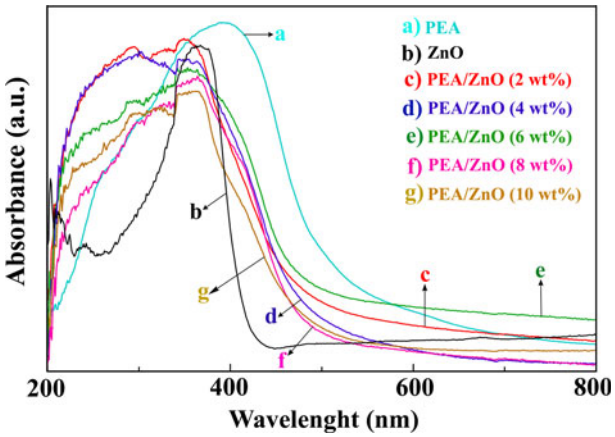

Fig. 9 UV/Vis spectra of modified ZnO, pure PEA, and PEA/ZnO BNCs

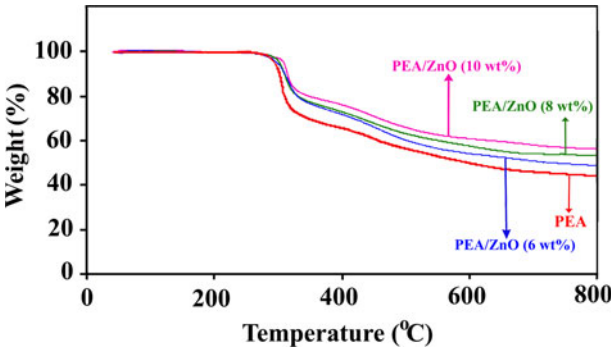

Fig. 10 TGA thermograms of PEA and PEA/ZnO BNCs (6, 8, and 10 wt%) under a nitrogen atmosphere at heating rate of 10 °C min^{-1}

addition of ZnO nanoparticles. After ultrasonication, the hydrogen bonding between PEA chains was decreased, so the T_g was reduced. Furthermore, the hydrogen bonding between PEA and ZnO increased, while the hydrogen bonding between PEA and PEA decreased after the addition of ZnO nanoparticles that caused the enhancement in the polymer chain mobility and decreasing in the T_g value. A single T_g was observed at lower than that of T_g of pure PEA confirms good dispersion of ZnO nanoparticles in polymer matrix and consequently good dispersion, causes increasing in amorphous structure due to decreasing in chain–chain interaction of polymer.

Conclusions

Novel polymer/ZnO nanocomposites based on optically active and biodegradable PEA were successfully synthesized through ultrasonication assisted process. Structural analysis confirmed the BNCs formation and it showed the relative

Table 1 Thermal properties of the PEA and PEA/ZnO BNCs

Polymer	Decomposition temperature (°C)		Char yield (%)[b]	LOI[c]
	T_5[a]	T_{10}[a]		
PEA	300	305	44	35.1
PEA/ZnO (6%)	302	307	49	37.1
PEA/ZnO (8%)	303	307	54	39.1
PEA/ZnO (10%)	305	309	58	40.7

[a] Temperature at which 5 and 10% weight loss were recorded by TGA at heating rate of 10 °C min^{-1} in a N_2 atmosphere

[b] Weight percent of the material left undecomposed after TGA at maximum temperature 800 °C in a N_2 atmosphere

[c] LOI evaluating char yield at 800 °C

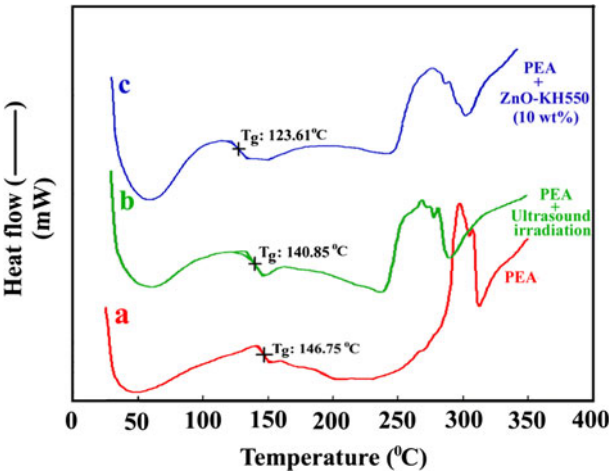

Fig. 11 DSC thermograms of (*a*) PEA, (*b*) PEA/ultrasound irradiation, and (*c*) PEA/ZnO-KH550 (10 wt%)

change in the peaks with increase in ZnO concentration. The FE-SEM, AFM, and TEM morphological analysis revealed the importance of silane coupling agent (KH550) on the surface of ZnO nanoparticles in controlling the size of ZnO nanoparticles. The existence of esteric C=O and amidic NH in polymer matrix, which were capable to interact with amine functional group and unmodified OH on the surface of ZnO via hydrogen bonding, improved the nanoparticles dispersion and shape as confirmed using morphology studies. In addition, incorporating nano-ZnO into PEA causes improvement in thermal stability of BNCs as was compared to the pure PEA.

Acknowledgments We gratefully acknowledge the partial financial support from the Research Affairs Division Isfahan University of Technology (IUT), Isfahan. Further partial financial support of Iran Nanotechnology Initiative Council (INIC), National Elite Foundation (NEF), and Center of Excellency in Sensors and Green Chemistry (IUT) is also gratefully acknowledged.

References

1. Berta M, Lindsay C, Pans G, Camino G (2006) Effect of chemical structure on combustion and thermal behaviour of polyurethane elastomer layered silicate nanocomposites. Polym Degrad Stab 91:1179–1191
2. Jordan J, Jacob KI, Tannenbaum R, Sharaf MA, Jasiuk I (2005) Experimental trends in polymer nanocomposites—a review. Mater Sci Eng A 393:1–11
3. Semaltianos NG, Logothetidis S, Hastas N, Perrie W, Romani S, Potter RJ, Dearden G, Watkins KG, French P, Sharp M (2010) Modification of the electrical properties of PEDOT:PSS by the incorporation of ZnO nanoparticles synthesized by laser ablation. Chem Phys Lett 484:283–289
4. Kumar AP, Depan D, Singh Tomer N, Singh RP (2009) Nanoscale particles for polymer degradation and stabilization—trends and future perspectives. Prog Polym Sci 34:479–515
5. Akamatsu K, Ikeda S, Nawafune H, Deki S (2003) Surface modification-based synthesis and microstructural tuning of nanocomposite layers: monodispersed copper nanoparticles in polyimide resins. Chem Mater 15:2488–2491
6. Byung-Yong L, Kris B, Murat Erdem K, Meghan Ann W-D, Richard FR, Yury G (2010) Titanium dioxide-coated nanofibers for advanced filters. J Nanopart Res 12:2511–2519
7. Savary E, Marinel S, Colder H, Harnois C, Lefevre FX, Retoux R (2010) Microwave sintering of nano-sized ZnO synthesized by a liquid route. Powder Technol 208:521–525
8. Hong RY, Qian JZ, Cao JX (2006) Synthesis and characterization of PMMA grafted ZnO nanoparticles. Powder Technol 163:160–168
9. Fernandes DM, Hechenleitner AAW, Lima SM, Andrade LHC, Caires ARL, Pineda EAG (2011) Preparation, characterization, and photoluminescence study of PVA/ZnO nanocomposite films. Mater Chem Phys. doi:10.1016/j.matchemphys.2011.03.002
10. Tjong SC, Liang GD (2006) Electrical properties of low-density polyethylene/ZnO nanocomposites. Mater Chem Phys 100:1–5
11. Yun S, Gadd G, Latella B, Lo V, Russell R, Holden P (2008) Mechanical properties of biodegradable polyhydroxyalkanoates/single wall carbon nanotube nanocomposite films. Polym Bull 61:267–275
12. Maurya A, Chauhan P (2011) Synthesis and characterization of sol–gel derived PVA-titanium dioxide (TiO_2) nanocomposite. Polym Bull 1–12. doi:10.1007/s00289-011-0589-6
13. Rajesh AhujaT, Kumar D (2009) Recent progress in the development of nano-structured conducting polymers/nanocomposites for sensor applications. Sens Actuators B 136:275–286
14. Sinha Ray S, Okamoto M (2003) Polymer/layered silicate nanocomposites: a review from preparation to processing. Prog Polym Sci 28:1539–1641
15. Singla M, Sehrawat R, Rana N, Singh K (2010) Dielectric behaviour of emeraldine base polymer–ZnO nanocomposite film in the low to medium frequency. J Nanopart Res 13:2109–2116
16. Mahdavian A, Sarrafi Y, Shabankareh M (2009) Nanocomposite particles with core–shell morphology III: preparation and characterization of nano Al_2O_3–poly(styrene–methyl methacrylate) particles via miniemulsion polymerization. Polym Bull 63:329–340
17. Wu YL, Tok AIY, Boey FYC, Zeng XT, Zhang XH (2007) Surface modification of ZnO nanocrystals. Appl Surf Sci 253:5473–5479
18. Chrissopoulou K, Anastasiadis SH (2010) Polyolefin/layered silicate nanocomposites with functional compatibilizers. Eur Polym J. doi:10.1016/j.eurpolymj.2010.09.028
19. Tang E, Cheng G, Ma X, Pang X, Zhao Q (2006) Surface modification of zinc oxide nanoparticle by PMAA and its dispersion in aqueous system. Appl Surf Sci 252:5227–5232
20. Grasset F, Saito N, Li D, Park D, Sakaguchi I, Ohashi N, Haneda H, Roisnel T, Mornet S, Duguet E (2003) Surface modification of zinc oxide nanoparticles by aminopropyltriethoxysilane. J Alloys Compd 360:298–311
21. Tang E, Liu H, Sun L, Zheng E, Cheng G (2007) Fabrication of zinc oxide/poly(styrene) grafted nanocomposite latex and its dispersion. Eur Polym J 43:4210–4218
22. Shi J, Wang Y, Gao Y, Bai H (2008) Effects of coupling agents on the impact fracture behaviors of T-ZnOw/PA6 composites. Compos Sci Technol 68:1338–1347
23. Okada M (2002) Chemical syntheses of biodegradable polymers. Prog Polym Sci 27(1):87–133
24. Nair LS, Laurencin CT (2007) Biodegradable polymers as biomaterials. Prog Polym Sci 32:762–798. doi:10.1016/j.progpolymsci.2007.05.017

25. Mallakpour S, Asadi P, Sabzalian MR (2010) Synthesis of biodegradable chiral poly(ester-imide)s derived from valine-, leucine- and tyrosine-containing monomers. Amino Acids. doi:10.1007/s00726-010-0799-5
26. Mallakpour S, Tirgir F, Sabzalian MR (2010) Synthesis and structural characterization of novel biologically active and thermally stable poly(ester-imide)s containing different natural amino acids linkages. J Polym Res 1–12. doi:10.1007/s10965-010-9427-z
27. Karimi P, Rizkalla AS, Mequanint K (2010) Versatile biodegradable poly(ester amide)s derived from α-amino acids for vascular tissue engineering. Materials 3:2346–2368
28. Tsitlanadze G, Kviria T, Katsarava R, Chu CC (2004) In vitro enzymatic biodegradation of amino acid based poly(ester amide)s biomaterials. J Mater Sci 15:185–190
29. Ozgur U, Alivov YI, Liu C, Teke A, Reshchikov MA, Dogan S, Avrutin V, Cho SJ, Morkoc H (2005) A comprehensive review of ZnO materials and devices. J Appl Phys 98:041103–041301
30. Gal D, Hodes G, Lincot D, Schock HW (2000) Electrochemical deposition of zinc oxide films from non-aqueous solution: a new buffer/window process for thin film solar cells. Thin Solid Films 361–362:79–83
31. Shouli B, Xin L, Dianqing L, Song C, Ruixian L, Aifan C (2010) Synthesis of ZnO nanorods and its application in NO_2 sensors. Sens Actuators B. doi:10.1016/j.snb.2010.10.010
32. Shi J, Cao Q, Wei Y, Huang Y (2003) ZnO varistor manufactured by composite nano-additives. Mater Sci Eng B 99:344–347
33. Wang Z (2009) Ten years' venturing in ZnO nanostructures: from discovery to scientific understanding and to technology applications. Chin Sci Bull 54:4021–4034
34. Saito N, Haneda H, Sekiguchi T, Ohashi N, Sakaguchi I, Koumoto K (2002) Low-temperature fabrication of light-emitting zinc oxide micropatterns using self-assembled monolayers. Adv Mater 14:418–421
35. Tu Y, Zhou L, Jin YZ, Gao C, Ye ZZ, Yang YF, Wang QL (2010) Transparent and flexible thin films of ZnO-polystyrene nanocomposite for UV-shielding applications. J Mater Chem 20:1594–1599
36. Katangur P, Patra PK, Warner SB (2006) Nanostructured ultraviolet resistant polymer coatings. Polym Degrad Stab 91:2437–2442
37. Kumar RTR et al (2007) Control of ZnO nanorod array density by Zn supersaturation variation and effects on field emission. Nanotechnology 18:215704
38. Nagai A, Ishikawa J, Kudo H, Endo T (2004) Synthesis of optically active polyurethanes by self-polyaddition of tyrosine-based monomers. J Polym Sci A 42:1143–1153. doi:10.1002/pola.11047
39. Abdolmaleki A, Mallakpour S, Borandeh S, Sabzalian MR (2011) Fabrication of biodegradable poly(ester-amide)s based on tyrosine natural amino acid. Amino Acids. doi:10.1007/s00726-011-0931-1
40. Impens NREN, van der Voort P, Vansant EF (1999) Silylation of micro-, meso- and non-porous oxides: a review. Microporous Mesoporous Mater 28:217–232
41. Chiang C-H, Ishida H, Koenig JL (1980) The structure of [gamma]-aminopropyltriethoxysilane on glass surfaces. J Colloid Interface Sci 74:396–404
42. Ukaji E, Furusawa T, Sato M, Suzuki N (2007) The effect of surface modification with silane coupling agent on suppressing the photo-catalytic activity of fine TiO_2 particles as inorganic UV filter. Appl Surf Sci 254:563–569
43. Krevelen DV, Hoftyzer P (1976) Properties of polymers, 3rd edn. Elsevier, Amsterdam